RESEARCH ARTICLE

Key Points:
- Lakewater temperature, turbidity, and bathymetry measured near large calving glaciers of the Southern Patagonia Icefield
- Thermal structure of the lakes characterized by wind-mixed warm water near the surface and cold/turbid glacial discharge near the bottom
- Cold water at pressure melting point fills lower half of the lake of Glaciar Viedma, affecting subaqueous melting of the ice front

Correspondence to:
S. Sugiyama,
sugishin@lowtem.hokudai.ac.jp

Thermal structure of proglacial lakes in Patagonia

Shin Sugiyama[1], **Masahiro Minowa[1,2]**, **Daiki Sakakibara[1,3]**, **Pedro Skvarca[4]**, **Takanobu Sawagaki[5]**, **Yoshihiko Ohashi[1,2]**, **Nozomu Naito[6]**, and **Kazuhisa Chikita[7]**

[1]Institute of Low Temperature Science, Hokkaido University, Sapporo, Japan, [2]Graduate School of Environmental Science, Hokkaido University, Sapporo, Japan, [3]Arctic Research Center, Hokkaido University, Sapporo, Japan, [4]Glaciarium-Glacier Interpretive Center, El Calafate, Argentina, [5]Faculty of Social Sciences, Hosei University, Tokyo, Japan, [6]Faculty of Environmental Studies, Hiroshima Institute of Technology, Hiroshima, Japan, [7]Faculty of Science, Hokkaido University, Sapporo, Japan

Abstract Calving glaciers are rapidly retreating in many regions under the influence of ice-water interactions at the glacier front. In contrast to the numerous researches conducted on fjords in front of tidewater glaciers, very few studies have been reported on lakes in which freshwater calving glaciers terminate. To better understand ice-water interactions at the front of freshwater calving glaciers, we measured lakewater temperature, turbidity, and bathymetry near Glaciar Perito Moreno, Upsala, and Viedma, large calving glaciers of the Southern Patagonia Icefield. The thermal structures of these lakes were significantly different from those reported in glacial fjords. There was no indication of upwelling subglacial meltwater; instead, turbid and cold glacial water discharge filled the region near the lake bottom. This was because water density was controlled by suspended sediment concentrations rather than by water temperature. Near-surface wind-driven circulation reaches a depth of ~180 m, forming a relatively warm isothermal layer (mean temperature of ~5–6°C at Perito Moreno, ~3–4°C at Upsala, and ~6–7°C at Viedma), which should convey heat energy to the ice-water interface. However, the deeper part of the glacier front is in contact with stratified cold water, implying a limited amount of melting there. In the lake in front of Glaciar Viedma, the region deeper than 120 m was filled entirely with turbid and very cold water at pressure melting temperature. Our results revealed a previously unexplored thermal structure of proglacial lakes in Patagonia, suggesting its importance in the subaqueous melting of freshwater calving glaciers.

1. Introduction

Out of 64 major outlet glaciers in the Northern and Southern Patagonia Icefields (NPI and SPI), more than 80% of the termini end in water [*Aniya*, 1988; *Aniya et al.*, 1996; *Rivera and Casassa*, 1999; *Rignot et al.*, 2003]. The majority of glaciers in the NPI and those located on the eastern side of the SPI flow into freshwater lakes, and these lake-calving glaciers account for ~70% of the calving glaciers in Patagonia [*Rignot et al.*, 2003]. Most of the glaciers in Patagonia have retreated in recent decades [*Aniya et al.*, 1997; *Davies and Glasser*, 2012; *Sakakibara and Sugiyama*, 2014; *White and Copland*, 2015]. Some glaciers in the SPI have retreated much more rapidly than others, as exemplified by the >6 km retreat of Glaciar Upsala, Jorge Montt, and HPS12 between 1984 and 2011 [*Sakakibara and Sugiyama*, 2014]. Such heterogeneous variations in retreat rates are observed commonly in other regions, including Greenland [e.g., *Moon and Joughin*, 2008] and Alaska [e.g., *McNabb and Hock*, 2014]. Rapidly retreating glaciers in Patagonia are also showing ice speed acceleration [*Sakakibara and Sugiyama*, 2014], implying a substantial increase in frontal ablation (calving plus subaqueous and subaerial frontal melting).

Frontal ablation plays a key role in calving glacier variations, which are generally more rapid than those of land-terminating glaciers. It was previously thought that frontal ablation occurs mostly by means of calving, but recent studies on tidewater glaciers in Greenland and Alaska have shown that the contribution of subaqueous melting is substantially larger than previously assumed [*Motyka et al.*, 2003, 2013; *Rignot et al.*, 2010; *Sutherland and Straneo*, 2012; *Bartholomaus et al.*, 2013]. For example, field measurements at Yahtse Glacier, a 2.7 km wide tidewater glacier in Alaska, showed that subaqueous melt rate was greater than $9 \, \mathrm{m \, d^{-1}}$ and this rate accounted for more than 50% of the ice velocity at the calving front [*Bartholomaus et al.*, 2013]. An increasing number of studies have been reported on ocean processes operating near the calving front, and these studies reveal the importance of thermal structure and circulation in fjords for submarine melting [e.g., *Jenkins*, 2011; *Sciascia et al.*, 2013; *Xu et al.*, 2013]. The connection of fjord

systems to the open ocean was also studied intensively in recent years [e.g., *Straneo et al.*, 2010; *Inall et al.*, 2014; *Jackson et al.*, 2014].

In contrast to the many research projects on tidewater glaciers and fjords, relatively few studies have been carried out on the interaction of freshwater calving glaciers and proglacial water systems. This is not because freshwater calving glaciers are less important in the context of recent glacier changes. Freshwater calving glaciers in the SPI and NPI are rapidly retreating, playing a central role in the recent ice mass loss in Patagonia [e.g., *Davies and Glasser*, 2012; *Willis et al.*, 2012; *Sakakibara and Sugiyama*, 2014]. Furthermore, some of the lake-calving glaciers in Alaska have shown more rapid changes than tidewater glaciers in the region [*Boyce et al.*, 2007; *Larsen et al.*, 2007, 2015; *Trüssel et al.*, 2013]. Moreover, the number of freshwater calving glaciers is increasing around the world due to proglacial lake formation following glacier retreat [e.g., *Carrivick and Tweed*, 2013]. For instance, lakes are increasing and expanding at the margins of the Greenland ice sheet, causing a potential impact on ice sheet mass loss [*Carrivick and Quincey*, 2014]. Formation and expansion of moraine-dammed lakes due to glacier retreat is of great concern in Asian high mountain regions [e.g., *Fujita et al.*, 2013; *Nie et al.*, 2013]. Therefore, it is increasingly important to study the lakes in front of calving glaciers and the processes occurring near the calving front in order to better understand the impact of lakes on glacier changes.

The circulation and thermal structure of water near freshwater calving glaciers are significantly different from those at tidewater glaciers [*Truffer and Motyka*, 2016]. In tidewater glaciers, subglacial meltwater discharge forms an upwelling current in a fjord because of the density difference between sea water and glacial meltwater. This buoyant discharge enhances melting at the calving front by incorporating warm ocean water into a plume, aiding the heat transfer from water to ice [*Motyka et al.*, 2003, 2013; *Jenkins*, 2011; *Xu et al.*, 2013]. This is not always the case for lake-calving glaciers. The behavior of subglacial meltwater once discharged into a lake is controlled by the density difference between glacial meltwater and lake water, which is dependent on temperature, pressure, and sediment concentration. In fresh water, buoyancy acting on subglacial discharge is much less than that in seawater as the density difference is small; for this reason, active upwelling and efficient heat exchange at the ice-water interface are unlikely. The heat source for melting in fresh water is also different from the one for submarine melting. Solar radiation energy is the most important heat source in a closed lake [*Funk and Röthlisberger*, 1989], whereas abundant heat is available in fjords via convection from the open ocean. It is hypothesized that the upwelling of subglacial discharge acts also as a pump to draw warm water from the open ocean into a fjord [*Gladish et al.*, 2015]. In Greenland, warm and salty Atlantic water intrudes into a fjord and forms a thick layer beneath relatively cold and fresh polar water [e.g., *Straneo et al.*, 2010]. Assuming a lack of circulation driven by subglacial discharge, lakewater temperature distribution is expected to be substantially different from such observations in Greenlandic fjords.

The water temperature of lakes in contact with a glacier front has been reported in several regions, including Alaska [*Josberger et al.*, 2006; *Boyce et al.*, 2007; *Trüssel et al.*, 2013], New Zealand [*Hochstein et al.*, 1995, 1998; *Warren and Kirkbride*, 2003], Himalaya [*Chikita*, 2007; *Chikita et al.*, 1999], and Patagonia [*Haresign and Warren*, 2005]. Most of the study results agree that proglacial lakes are filled with cold water, often colder than 1℃ [*Truffer and Motyka*, 2016]. In Alaska, the temperature of the lakes was colder than 3℃ in front of Mendenhall [*Boyce et al.*, 2007], Yakutat [*Trüssel et al.*, 2013], and Bering Glaciers [*Josberger et al.*, 2006], except for near-surface shallow layers. These temperatures are significantly lower than that of sea water in front of tidewater glaciers in the same region [*Truffer and Motyka*, 2016]. Similar results have been reported in other regions. In New Zealand, lakewater temperature in front of Tasman Glacier was below 1℃ [*Hochstein et al.*, 1995], and it varied from 3℃ near the surface to <1℃ at the lake bottom in front of Hooker Glacier [*Hochstein et al.*, 1998]. Lake water in front of Glaciar León in the SPI was substantially warmer (~5℃) than the above examples, which can be attributed to the large size of the lake (Lago Leones) (~20 km^2) and relatively low latitude (46° S) and altitude (303 m) [*Haresign and Warren*, 2005]. It should be noted also that Glaciar León was partly cut off from the lake and in contact with water over a relatively small area (glacier width of ~1.5 km and mean water depth of 65 m) [*Haresign and Warren*, 2005]. Therefore, the influence of glacier-lake interaction on the thermal condition of Lago Leones is expected to be small. Glaciers in the SPI flow into much larger lakes such as Lago Argentino (~1480 km^2) and Viedma (~1100 km^2), but no measurements have been reported in these lakes near the fronts of calving glaciers.

To better understand the interaction between freshwater calving glaciers and lakes, we performed lake measurements in front of three large glaciers in the SPI, i.e., Glaciar Perito Moreno (GPM), Glaciar Upsala (GU), and

Glaciar Viedma (GV). Water temperature and turbidity profiles were obtained by lowering sensors at several locations, and lake bathymetries were surveyed using an ultrasonic echo sounder. The results were analyzed to show the thermal structure of ~100–600 m deep lakes. Based on the observational results, we discuss processes controlling the thermal structure of these lakes and their influence on subaqueous melting of the glaciers.

2. Study Site

2.1. Glaciar Perito Moreno

GPM is located in the southeastern part of the SPI (50.5°S, 73.1°W), covering an area of 259 km^2 [*De Angelis*, 2014] (Figure 1). The glacier flows into the southwestern channel of Lago Argentino at an altitude of ~178 m above sea level (asl). The glacier front crosses the channel and extends to the opposite shore at Peninsula Magallanes, forming an ice barrier which separates the lake into Brazo Rico (BR) to the south and Canal de los Témpanos (CT) to the north (Figure 2a). The calving front is about 5 km long in total, and its southern and northern sections face these two arms of Lago Argentino, respectively. According to previous water depth soundings near the calving front, maximum depth in BR near the glacier was ~110 m and that in CT ~164 m [*Stuefer et al.*, 2007]. Lake water usually flows from BR to CT through a narrow channel between the ice front and the peninsula, but a small advance of the glacier causes occasional formation of an ice dam. More than 20 damming and outburst events have been observed since the 1910s with irregular intervals [*Skvarca and Naruse*, 2006; *Stuefer et al.*, 2007].

In contrast to other rapidly retreating glaciers in the SPI, GPM has shown no significant changes in the terminus position and ice surface elevation in recent decades [*Minowa et al.*, 2015]. Ice surface elevation has been fairly stable since 1990, and the front position has varied only within several hundred meters since 1920 [*Skvarca and Naruse*, 1997]. The ice front position shows seasonal variations [*Minowa et al.*, 2015], which affect the width of the channel connecting BR and CT. Ice speeds averaged along each section of the calving front facing BR and CT are 800 and 470 m a^{-1}, which generate ice discharge into the lake of 95 and 280 × 10^9 kg a^{-1}, respectively [*Rott et al.*, 1998]. Annual mean ice speed has shown little change since the 1980s [*Sakakibara and Sugiyama*, 2014], but seasonal and shorter-term speed variations are reported in the ablation area [*Ciappa et al.*, 2010; *Sugiyama et al.*, 2011].

2.2. Glaciar Upsala

Glaciar Upsala (GU) is situated on the eastern side of the SPI (49.9°S, 73.3°W) at about 70 km north of GPM (Figure 1). In 2011, the glacier had an area of 840 km^2 and length of 54 km [*Sakakibara et al.*, 2013], making it the fourth largest glacier in the SPI [*De Angelis*, 2014]. Ice flows southward into Brazo Upsala (BU), a northwestern arm of Lago Argentino. Connecting CT, BR, BU, and several other arms, Lago Argentino forms one of the largest lakes in Patagonia (~1480 km^2), which feeds into the Atlantic Ocean through 385 km long Santa Cruz River [*Pasquini and Depetris*, 2011]. In 2010, the calving front of GU was ~3.0 km wide and the ice cliff was ~50 m above the lake surface [*Sakakibara et al.*, 2013]. According to measurements performed in the 1990s, the lake is 600 m deep at about 4 km from the 2014 glacier terminus [*Naruse and Skvarca*, 2000].

GU is one of the most rapidly retreating glaciers in the SPI in the last decades. The glacier front receded by 7 km from 1984 to 2011, which includes the disintegration of the lower 3 km of ice during the 2008–2011 period [*Sakakibara et al.*, 2013]. The front position has been relatively stable since then, located at the confluence with Glaciar Bertacchi in 2014 (Figure 2b). During the rapid retreat in 2008–2011, substantial acceleration was observed in the lower reaches of the glacier. After an approximately twofold speed increase, ice speed near the front was greater than 3 km a^{-1} in 2011 [*Muto and Furuya*, 2013; *Sakakibara and Sugiyama*, 2014].

2.3. Glaciar Viedma

Glaciar Viedma (GV) is the second largest glacier in the SPI with an area of 974 km^2. The glacier flows eastward from the icefield and drains into Lago Viedma (LV) at 49.5°S and 73.0°W about 50 km north from GU (Figure 1). GV is the only glacier calving into LV, which has an area of approximately 1100 km^2 and feeds into Lago Argentino through La Leona River. GV calves directly into the main basin of the lake, unlike GPM and GU which flow into the narrow arms west of Lago Argentino. A large drainage basin of GV converges toward the terminus and discharges ice through a relatively narrow (1.5 km) calving front (Figure 2c). Lake depth near the glacier has never been reported. GV has been retreating at a steady rate in recent decades. Retreat
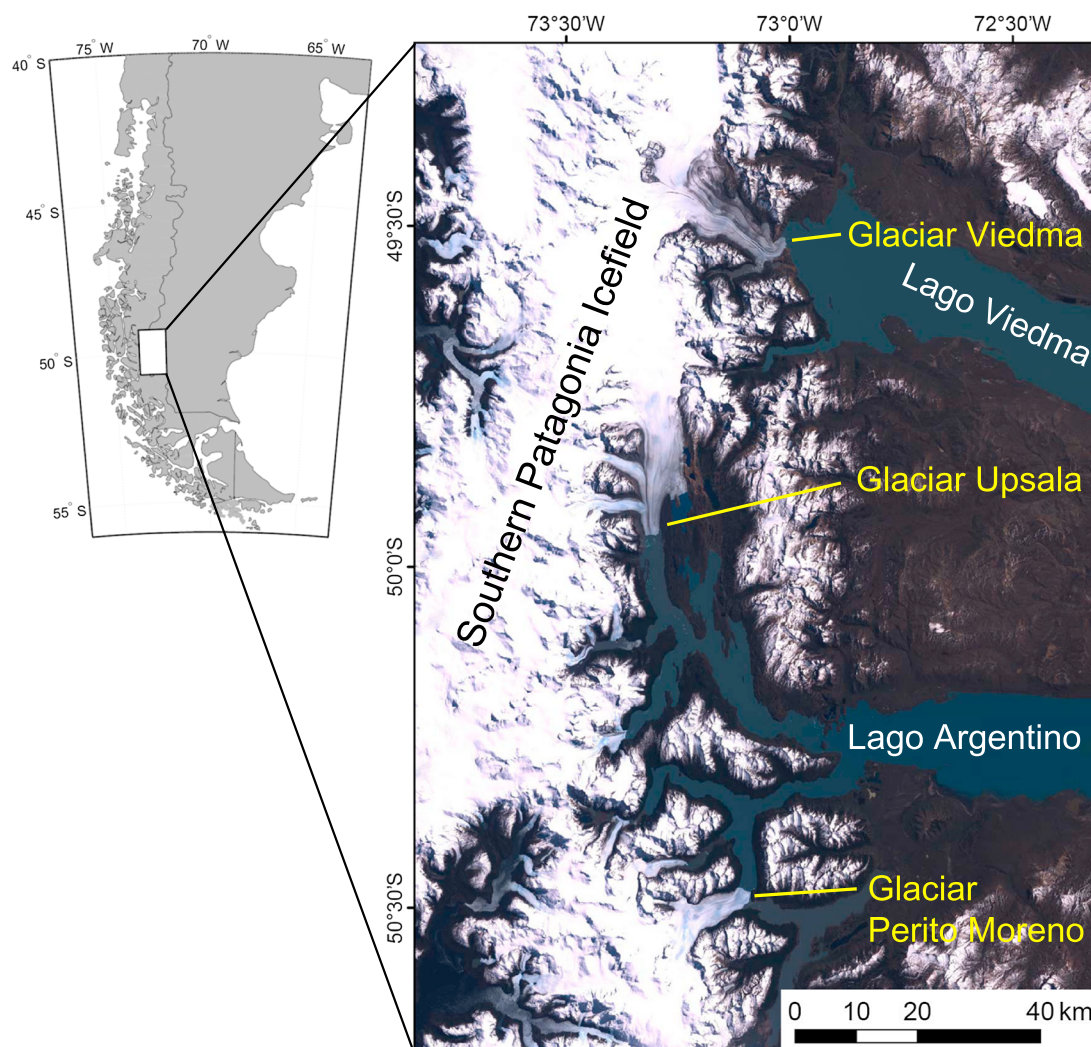
Figure 1. Satellite image (Landsat 7, 14 October 2001) showing the studied glaciers and lakes in the central part of the SPI. The inset shows the location of the study site in South America.

distance from the 1980s to 2011 was about 1 km [*Sakakibara and Sugiyama*, 2014]. Ice flows at a rate of 600–700 m a^{-1} near the calving front, and this rate has been stable since the 1980s [*Sakakibara and Sugiyama*, 2014].

3. Methods

3.1. Water Depth

Water depth was measured in December 2012 (LV), December 2013 (BR, CT, BU, and LV), and October 2014 (BU) within 3–4 km from the calving fronts of the glaciers (Figure 2). We used an ultrasonic echo sounder (Lowrance HDS-5 Gen2) operated with 200 kHz (Lowrance HST-DFSBL) or 50 kHz transducers (Airmar P319) mounted on a boat. Depth was determined automatically and recorded by the sounder every 1 s, while the boat was operated at a speed of approximately 10 km h^{-1}. The depth data were synchronized with horizontal coordinates obtained using a built-in GPS (global positioning system) of the sounder.

The accuracy of the echo sounding was determined by comparing the sounder data with that obtained by means of the water property profiler described below. According to the comparisons at 20 locations with depths ranging from 28 to 554 m, the mean error was 5.7 m or 3.7% of the depth. Errors in the GPS single positioning are expected to be several meters in the horizontal direction.
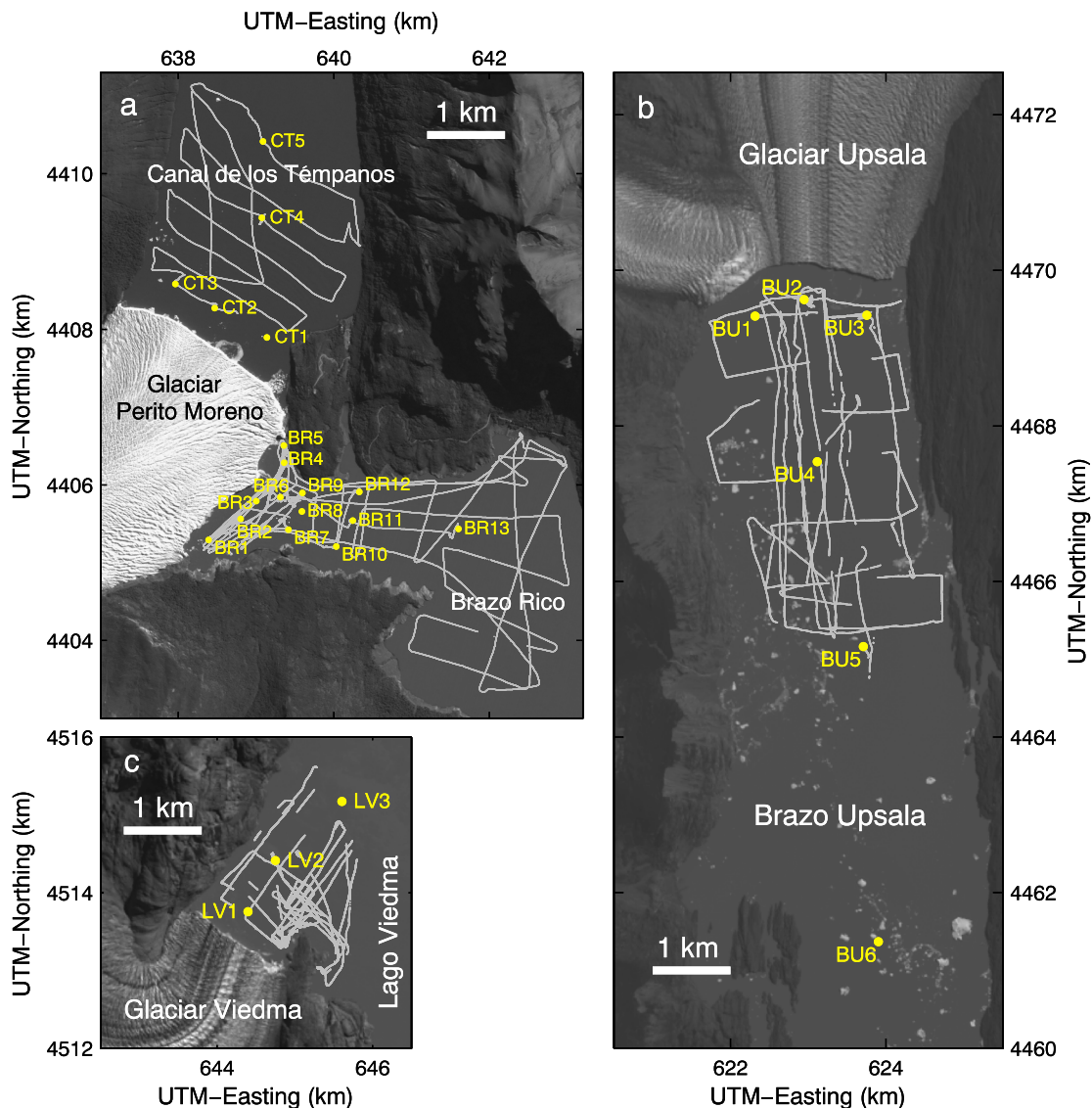
Figure 2. (a) Satellite image (ALOS PRISM, 19 July 2011) showing the calving front of GPM and measurement sites in BR and CT. Lakewater temperature and turbidity measurement sites are shown by dots, and the bathymetry survey tracks are indicated by gray lines. (b) Satellite image (Landsat 8, 12 February 2014) showing the calving front of GU and measurement sites in BU. (c) Satellite image (Landsat 8, 28 February 2014) showing the front of GV and measurement sites in LV.

3.2. Water Temperature and Turbidity

In austral summer 2013, we measured lakewater temperature and turbidity in front of the three calving glaciers. The measurements were performed on 6, 7, and 30 December at 13 locations in BR (Figure 2 a), on 19 December at 5 locations in CT (Figure 2a), on 18 December at 6 locations in BU (Figure 2b), and on 29 and 30 December at 3 locations in LV (Figure 2c). A temperature, turbidity, and depth profiler (JFE Advantec, ASTD101) was lowered from the boat to record the water properties every 1 s, except for the sites BR1–BR5 where data were recorded every 1 m. The sampling interval (1 s) was equivalent to resolutions of 0.2–1 m in depth. The accuracy of the depth, temperature, and turbidity measurements were ± 1.8 m, $\pm 0.01°C$, and ± 0.3 FTU (formazin turbidity unit) or 2% of measured turbidity, respectively.

The turbidity measured by the profiler was converted to suspended sediment concentration (SSC), based on a linear relationship obtained by filtering water samples collected in BR (Figure 3). We sampled water at three different depths near the glacier front at BR3 (Figure 2a). The SSC of each sample was obtained by weighing
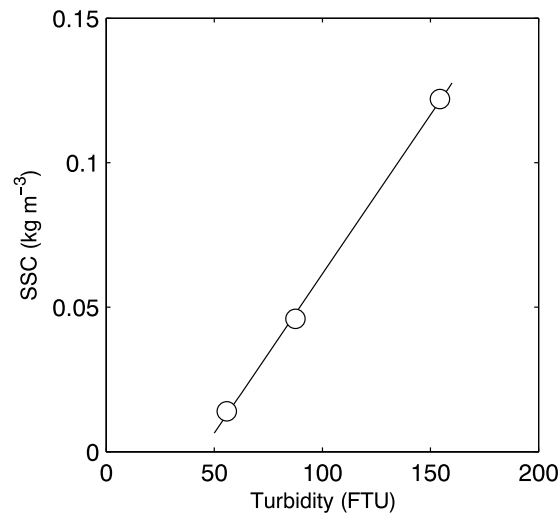
Figure 3. Relationship between turbidity obtained in the field with a profiler and SSC measured by filtering water samples.

sediments filtered with millipore filters of 0.45 μm opening. The bulk density of lake water ρ (kg m^{-3}) at 1 atm is given by

$$\rho(T, C) = \left(1 - \frac{C}{\rho_s}\right) \times \rho(T) + C \qquad (1)$$

where C (kg m^{-3}) is SSC, ρ_s (kg m^{-3}) is the density of suspended particles, and ρ (T) (kg m^{-3}) is pure water density at temperature T (°C). We used a particle density of 2730 kg m^{-3}, a value reported for sediment sampled in a proglacial lake in Nepal [*Chikita et al.*, 1999], since no data were available for the studied lakes. Lakewater density at a measurement depth ρ (T, C, P) was obtained by taking the compressibility of water (4.6 × 10^{-10} Pa^{-1}). We also used the residual density $\sigma = [\rho(T, C, P) - 1000] \times 10$ to present data.

4. Results

4.1. Glaciar Perito Moreno

4.1.1. Bathymetry

Lake depth measurements in front of GPM showed contrasting bed geometry in BR and CT (Figure 4a). The bed of BR forms a V-shaped valley with a relatively rugged topography. The lake is shallower than 70 m near the front of the glacier, and it deepens to ~100 m at about 500 m from the ice front (Figure 4a). The bed is flat in this region, suggesting deposition of glacial sediments. The lake gradually deepens from this point toward a 170 m deep basin at about 3 km from the glacier. The bed slope is steep across the valley, forming a relatively narrow channel. The bed of CT is U shaped, i.e., it consists of a large flat central area and steep side walls (Figure 4a). The central area is 160–180 m deep, and the bed is fairly flat. The lake bottom geometry suggests that CT had been more heavily eroded by glacial processes as compared to BR and covered with glacial sediments.

4.1.2. Water Temperature and Turbidity

In BR, water temperature and turbidity distributions were relatively uniform with depth and between the survey sites (Figure 5). Water temperature was ~6°C near the surface, and it gradually decreased to 4–5°C toward the bottom. Full depth averaged water temperature at each of the 13 measurement sites (BR1–BR13) was within a range between 5.38 and 5.71°C with a mean of 5.49°C. The upper 10 m mean temperature averaged over the 13 sites was 6.09°C, which was about 1°C warmer than the lower 10 m mean temperature (5.05°C). Water was more turbid in the deeper regions, particularly at depths greater than 50 m (Figure 5). Turbidity averaged within the lower 10 m over the 13 sites (129 FTU) was about two times greater than the value in the upper 10 m (62 FTU). These trends in temperature and turbidity were uniformly observed over the survey area in BR. For example, measurements in the central part of the lake at BR8 and BR11 were very similar to those obtained near the lake margins at BR7/9 and BR10/12, respectively (Figures 5c and 5d). The only exception is BR1, the site in front of the glacier terminus near the southern margin (Figure 2a). Within the 28 m deep water, a thermocline was observed at about 5 m from the bottom (Figure 5f). The lower layer was filled with colder (~4°C) and more turbid water, suggesting the influence of subglacial meltwater discharge or a stream running near the glacier margin.

In CT, on the northern side of GPM calving front, water temperature was similar to that observed in BR except for a relatively warm layer near the surface (Figure 6). Upper and lower 10 m mean temperatures over the surveyed area were 7.52 and 5.35°C, respectively. Full depth mean temperature averaged over the five survey sites (CT1–CT5) was 5.94°C, which was ~0.5°C warmer than the mean temperature in BR. Water in CT was generally less turbid than in BR. In the upper 10 m, mean turbidity in CT (24 FTU) was 40% of that in BR. Turbidity
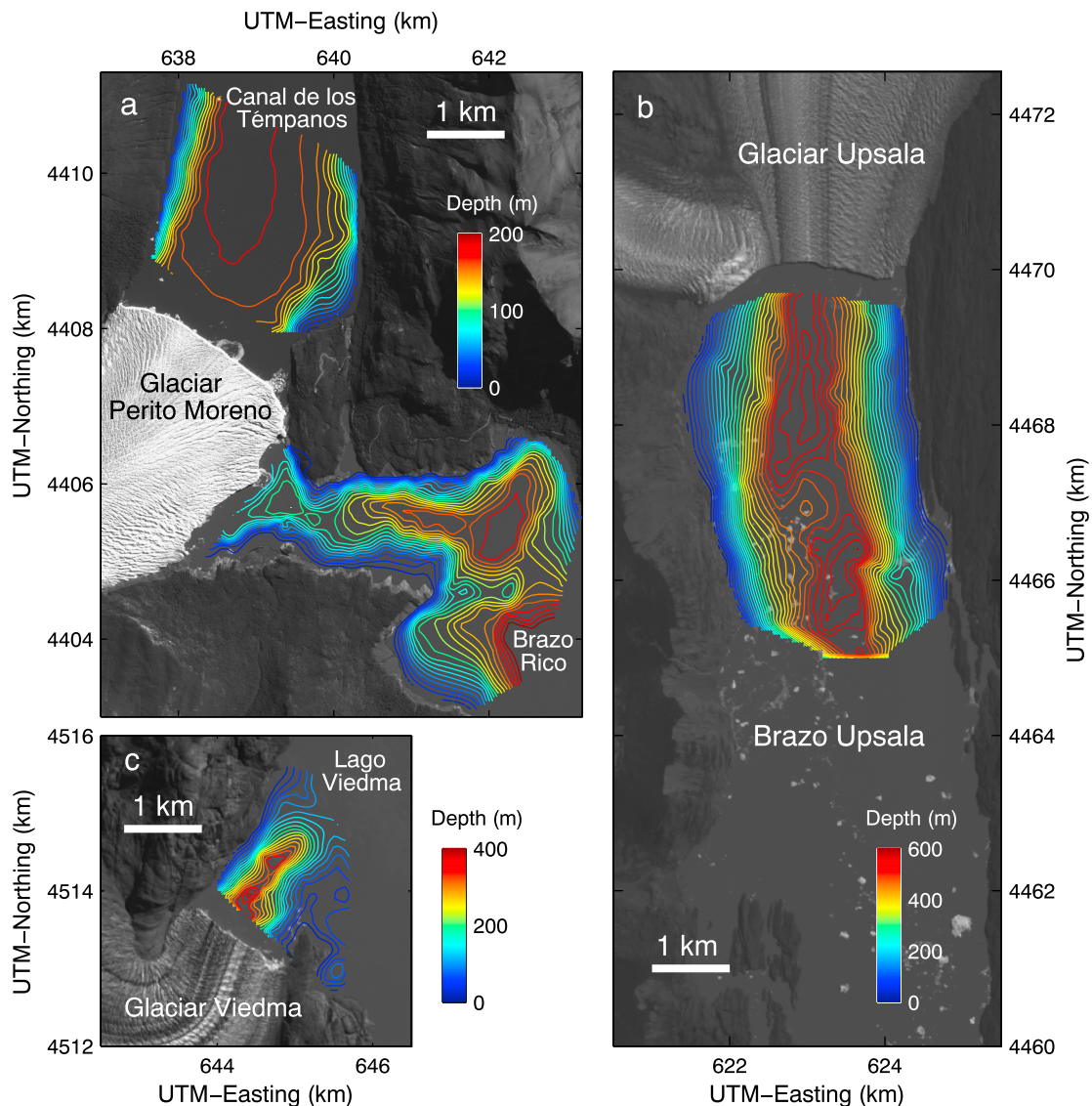
Figure 4. Water depth of (a) BR and CT, (b) BU, and (c) LV. Contour intervals are 10 m for Figures 4a and 4c and 20 m for Figure 4b. Background images are ALOS PRISM acquired on 19 July 2011 (Figure 4a), Landsat 8 on 12 February 2014 (Figure 4b), and Landsat 8 on 28 February 2014 (Figure 4c).

increased in the deeper regions and sharp peaks were observed near the bottom, but the lower 10 m mean value (75 FTU) was about 60% of the value in BR. These properties were uniformly distributed over the lake. Along the calving front (CT1–CT3), temperature and turbidity profiles were nearly identical to each other (Figure 6a). There were no clear indications of subglacial water discharge from the glacier.

4.2. Glaciar Upsala
4.2.1. Bathymetry
Our measurements revealed the bathymetry of BU in regions recently exposed by the rapid glacier retreat from 2008 onward. BU is 560–580 m deep along the valley (Figure 4b). The valley center was relatively narrow within ~1 km from the glacier front, and then it widened down the valley and formed a 1 km wide trough with several bumps and ridges. The depth at the lake center and the shape of the valley cross section were consistent with the previously reported geometry of BU south of our study site [*Naruse and Skvarca*, 2000].
4.2.2. Water Temperature and Turbidity
Water properties in front of GU were significantly different from those observed at GPM. Near the center of the calving front at BU2 (Figure 2b), the water temperature profile showed a stratified structure that consisted of three distinctive layers (Figure 7a). Temperature within several meters of the surface was 4.5–5°C, then
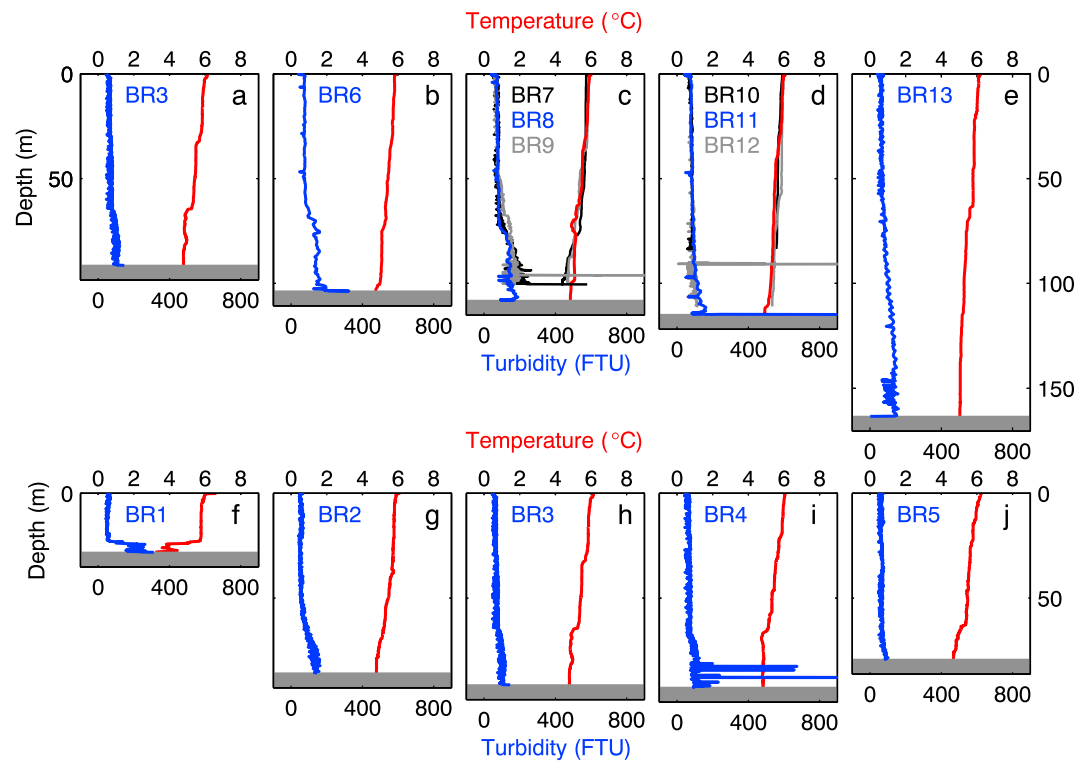
Figure 5. Water temperature (red) and turbidity (blue) profiles obtained in BR at measurement sites (BR1–BR13) shown in Figure 2a.

dropped to about 3.5°C at the depth of 40 m. Below this depth, the temperature was fairly uniform down to the depth of 180 m and ranged from 3.25 to 3.61°C with a mean of 3.45°C. Water temperature then gradually decreased from 180 to 280 m until reaching a homogeneous layer lying between 280 and 470 m depth. The temperature ranged from 1.66 to 2.06°C within this 190 m thick water layer. Cold water (0.56–0.80°C) formed the third and the final isothermal layer, filling the deepest part of the lake (>490 m). Turbidity variations at BU2 were associated with the temperature structure (Figure 7a). Turbidity was relatively uniform within the upper (40–180 m) and middle (280–470 m) isothermal layers with mean values of 109 and 298 FTU, respectively. Highly turbid water was found in the bottom layer, where mean turbidity from 490 m to the lake bottom (554 m) was 609 FTU.

Near the lake margins at BU1 and BU3, water temperature and turbidity in the upper 300 m were very similar to those at the lake center (Figure 7a). This indicates that water properties were uniformly distributed along
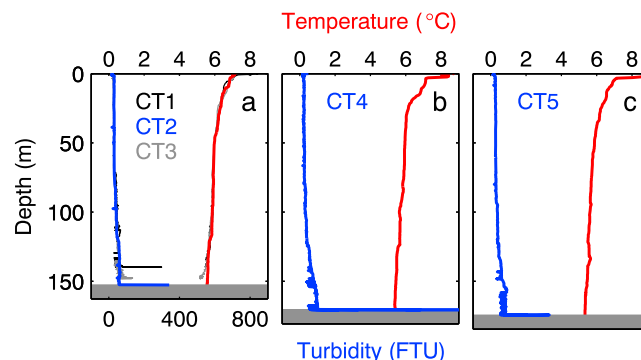

Figure 6. Water temperature (red) and turbidity (blue) profiles obtained in CT at measurement sites (CT1–CT5) shown in Figure 2a.
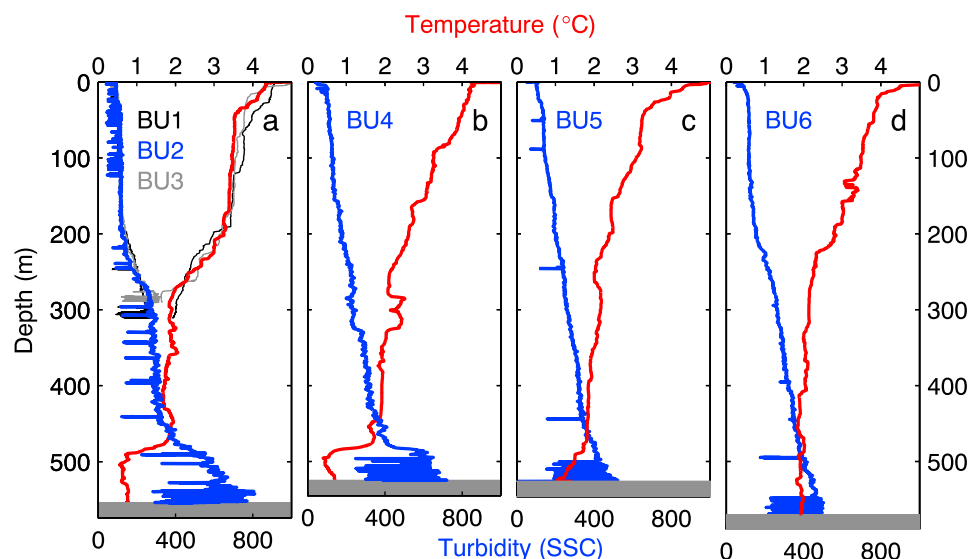
Figure 7. Water temperature (red) and turbidity (blue) profiles obtained in BU at measurement sites (BU1–BU6) shown in Figure 2b.

the calving front in a horizontal plane. The vertical stratification progressively weakened away from the glacier. The upper layer was indiscernible at 2.5 km from the glacier front (BU4, Figure 7b), and the middle layer was unclear at 5 km (BU5, Figure 7c). At 8.5 km from the glacier, the turbid bottom layer could be distinguished, but temperature was fairly uniform at the depth deeper than 400 m and the cold water ($< \sim 1°C$) was not observed near the bottom (BU6, Figure 7d). Full depth mean temperature and turbidity averaged along the centerline (BU2 and BU4–BU6) were 2.46°C and 249 FTU, respectively. Thus, lake water in front of GU was substantially colder and more turbid than that in front of GPM.

4.3. Glaciar Viedma

4.3.1. Bathymetry

The maximum depth of LV within our survey area was ~390 m at 500 m from the front of GV (Figure 4c). A trough extended from this point off the glacier to the next depression (360–370 m deep) at about 1 km from the ice front. This trough was located closer to the western margin and bounded by a steep side wall to the northwest and a relatively gently inclined bed to the southeast (Figure 4c). From the second depression, the water depth progressively decreased down the valley. The lake was only 137 m deep at the LV3 measurement site (Figure 2c) about 2 km from the glacier front. The shallow bed in this region formed a sill diagonally crossing the trough, which is presumably associated with the ridge extending from the eastern flank of the glacier. Satellite images (Landsat TM and JERS-1 OPS) show that the glacier front was stable on this sill from 1984 to 1993, suggesting the influence of bed geometry on the glacier retreat.

4.3.2. Water Temperature and Turbidity

Measurements in LV in front of GV showed very clear two-layer stratifications in temperature and turbidity (Figure 8). Near the calving front of GV at LV1 (Figure 2c), temperature dropped sharply by 4.5°C within a meter at the depth from 118 to 119 m, and turbidity increased by 350 FTU at the same depth (Figure 8a). Cold (−0.2 to 1°C) and turbid (260–700 FTU) water entirely filled the depth below this thermocline. In the deeper region of this lower layer, temperature gradually decreased from −0.125°C at 175 m deep to −0.213°C at 300 m, which is approximately consistent with the pressure dependent melting point of freshwater with a linear coefficient of $-0.074 \, \mathrm{K \, MPa^{-1}}$ [*Petrenko and Whitworth*, 1999] (Figure 8b). Within this region, the root-mean-square deviation of the measured temperature from the linear relationship was 0.011°C.

The strong stratification was consistently observed at two other survey locations. Thermocline existed at a depth of 119–120 m at 1 km from the calving front (LV2, Figure 8c). Temperature fluctuated within $1 \pm 0.5°C$ at the depth of 120–170 m, and the region below this transition zone was filled with cold and turbid water with a mean temperature and turbidity of −0.20°C and 599 FTU. Water depth showed a local maximum
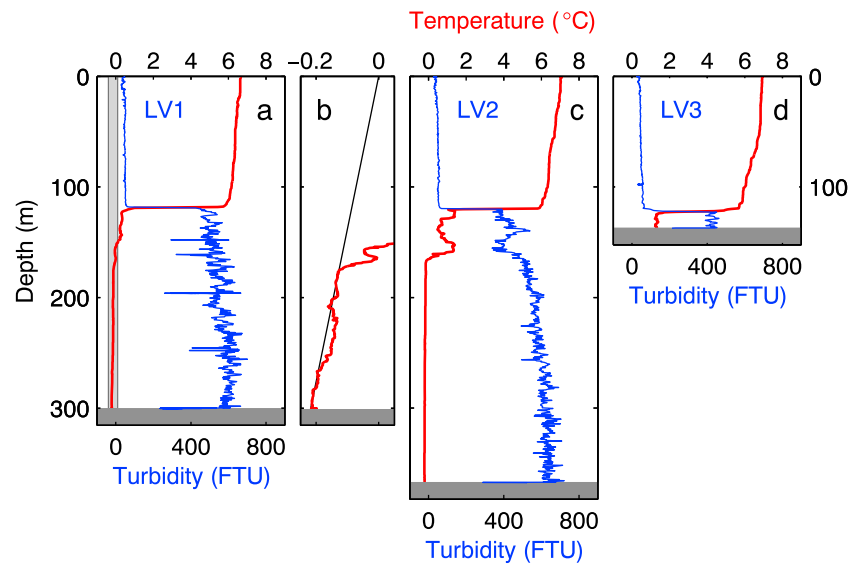
Figure 8. (a, c, and d) Water temperature (red) and turbidity (blue) profiles obtained in LV at measurement sites (LV1–LV3) shown in Figure 2c. (b) Details of the temperature profile at LV1 (same data as in Figure 8a) (red), and freezing temperature (black) computed with a linear pressure dependence of $-0.074\,\mathrm{K\,MPa}^{-1}$.

at around LV2 (367 m deep), and from this region the bed ascended steeply down the valley toward LV3, where the water depth was only 137 m. Jumps in the temperature and turbidity were still observed at LV3 at the depth of 119–123 m (Figure 8d), and this depth agreed with the thermocline observed at LV1 and LV2 within several meters. Within the 13 m thick water layer between the thermocline and the bed, mean temperature and turbidity were 1.32°C and 425 FTU, respectively.

Above the thermocline, the upper half of the lake was filled with homogeneously distributed warm and clean water. In this upper layer above the depth of 118 m, depth- averaged temperatures and turbidities at LV1–LV3 were within 6.3–6.6°C and 47–48 FTU, respectively.

5. Discussion

5.1. Lakewater Structure

5.1.1. Glaciar Perito Moreno

The lake water in front of GPM is characterized by uniformly distributed relatively warm water. Temperature distributions within the vertical cross sections along the centerlines of BR and CT show that the temperature gradient from the surface to the bottom is small except for the near-surface layer in CT (Figures 9a and 9b). The most likely interpretation of the fairly uniform temperature is that vertical water mixing is active from the lake surface to the bottom under the influence of persistently blowing strong wind in Patagonia. Wind in Patagonia is strong, particularly in summer. According to the observations near the terminus of GPM, wind speed varies between 3.7 and 7 m s^{-1} within a single day during summer [*Stuefer*, 1999]. Our data indicate that this wind is strong enough to overcome the stability in density stratification represented by the Brund-Väisälä frequency defined by $N^2 = (g/\rho)/(\mathrm{d}\rho/\mathrm{d}z)$ (Figures 10b and 10d), and it builds up vertical circulation near to the lake bottom.

Lake water was slightly colder (Figure 11a) and more turbid (Figure 11b) in BR than in CT. These differences arose because BR is situated upstream of the Lago Argentino lake system (Figure 1). Water flows from BR to CT through the narrow channel between the ice front and Peninsula Magallanes, whereas CT is directly connected to the main body of Lago Argentino. Accordingly, cold and turbid glacial meltwater in BR tends to stay near the glacier front for a longer period than in CT. SSC in CT was very low except for the water near the bottom (Figure 11b), suggesting that turbid glacial water drains from the glacier bed and flows away swiftly before it mixes with lake water. Such a regime of subglacial discharge is in contrast to that assumed in tidewater calving glaciers. When subglacial meltwater is discharged into the ocean, water upwells and forms a plume in front of the glacier [e.g., *Motyka et al.*, 2003]. Here our results indicated that discharge into the lake
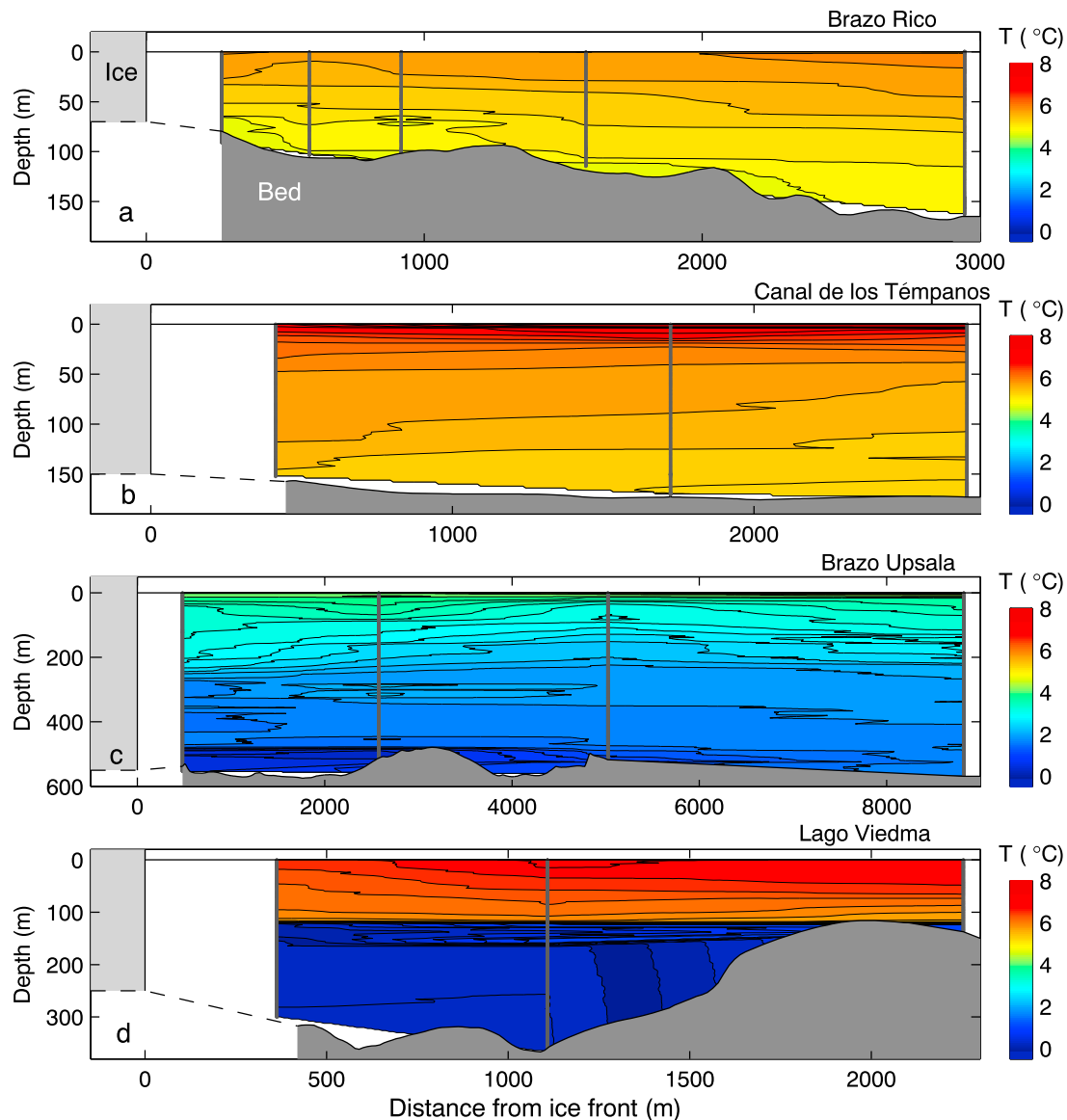
Figure 9. (a) Lakewater temperature in BR within a vertical cross-section along the center line connecting the sites BR3-BR6-BR8-BR11-BR13 (Figure 2a), (b) temperature in CT along CT2-CT4-CT5 (Figure 2a), (c) temperature in BU along BU2-BU4-BU5-BU6 (Figure 2b), and (d) temperature in LV along LV1-LV2-LV3 (Figure 2c). Contour intervals are 0.2°C. The glaciers and lake beds are indicated by the colors light and dark gray, respectively.

stays near the lake bottom since highly turbid subglacial meltwater is denser than lake water. Turbid bottom water was also found in BR (Figures 5f and 5i), and more clearly observed in BU and LV as described later. In general, water is less turbid in BR and CT than in BU and LV. This is probably because GPM has a smaller ablation area ($78 \, km^2$) as compared to GU ($226 \, km^2$) and GV ($321 \, km^2$) [*De Angelis*, 2014], and thus meltwater production and discharge from the terminus is less than for the other two glaciers.

5.1.2. Glaciar Upsala

If we compare temperature within the upper 100 m, water in BU was the coldest among the studied lakes (Figure 9c). This is consistent with a large amount of ice discharge due to the fast ice flow of GU [*Sakakibara et al.*, 2013]. Water temperature near the surface was 2–3°C colder than in other two lakes (Figure 11a), which we attribute to the influence of iceberg melting. The water temperature should be affected also by meltwater discharge from the glacier. A large volume of meltwater runoff is expected from the ablation area, extending over $226 \, km^2$ and 180–1170 m asl. Influence of meltwater discharge on the lake water was observed also in the magnitude of SSC, which was substantially greater than observed at BR and CT (Figure 11b).
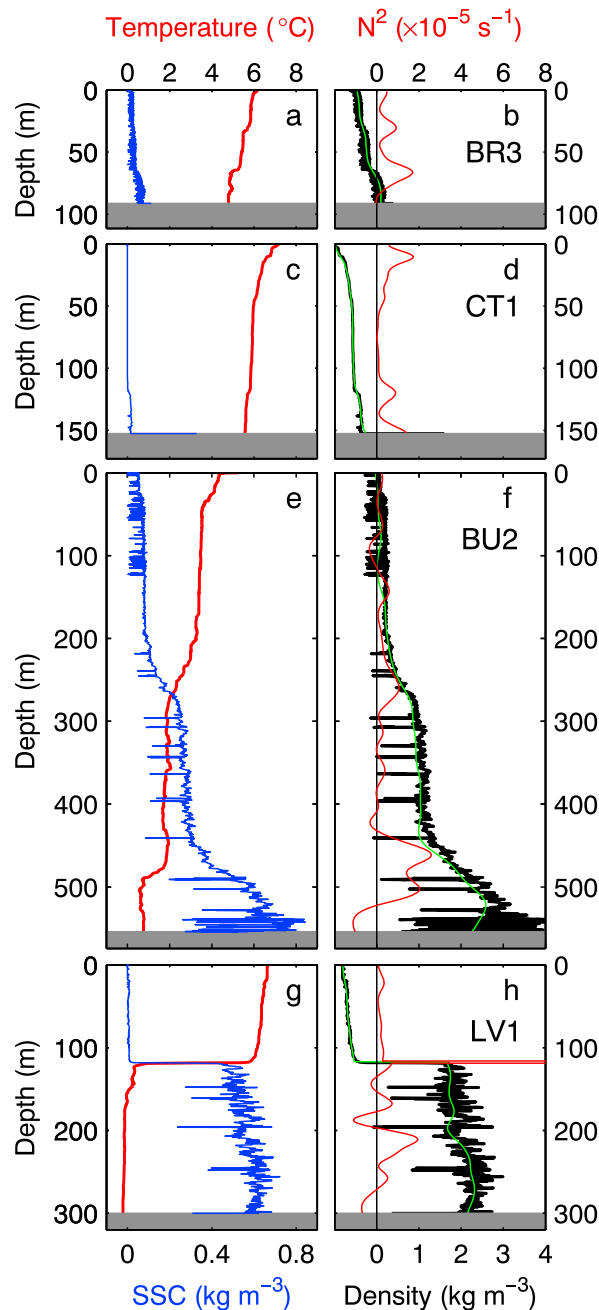
Figure 10. (a) Water temperature (red) and SSC (blue), and (b) Brund-Väisälä frequency (red) and the residual density (black) obtained at BR3 (Figure 2a). The green curve in Figure 10b was obtained by filtering the residual density. The same plots as Figures 10a and 10b but for the data obtained at (c, d) CT1, (e, f) BU2, and (g, h) LV1 (Figure 2).

The stratification of lake water in BU (Figures 7 and 9c) is explained in the following manner. Below the near-surface layer, which is directly influenced by heat exchange with the atmosphere, the upper homogeneous temperature layer (40–180 m) is formed as a result of wind-driven water circulation. The Brund-Väisälä frequency is close to zero from the surface to the depth of 200 m, implying active water mixing in this layer (Figure 10f). The cold and turbid bottom layer found deeper than 490 m is formed by subglacial meltwater discharge. Subglacial meltwater is dense because of high sediment concentration and thus stays near the lake bottom after discharge. The upper boundary of this bottom layer was ~500 m deep, which is approximately the same depth as the top of the bedrock bump at around 3 km from the glacier front (Figure 9c). The Brund-Väisälä frequency is large in the vicinity of this upper boundary, indicating the stability of stratification (Figure 10f). Down the valley from this bump, the dense and cold bottom water layer is not clearly distinguished (Figures 7 and 9c). Subglacial water fills the basin between the glacier and the bump and diffuses when it overtops the bump and flows to the lower reaches. Storage of sediment-laden water near the bed of a lake and its flow over a subaqueous sill were observed in a glacier-fed lake in Canada [*Chikita et al.*, 1996]. Between the upper and bottom water layers, the middle layer at the depth of 280–470 m shows fairly uniform temperature and SSC. We suggest that this layer is formed by circulation induced by both the wind-driven surface circulation and the subglacial discharge.

Active mixing within this layer is likely because the Brund-Väisälä frequency in this depth range is near zero and thus the density stratification is weak (Figure 10f). Water density variation from the surface to the bottom is consistent with the stepwise increase in the SSC profile (Figures 10e and 10f). This clearly indicates that the stability of the stratification in BU is governed by the sediment concentrations and not by water temperature.

5.1.3. Glaciar Viedma

The clear two-layer stratification observed in LV (Figure 9d) is intriguing. The density stratification is essentially controlled by the high sediment concentration in the lower layer, although temperature also shows a
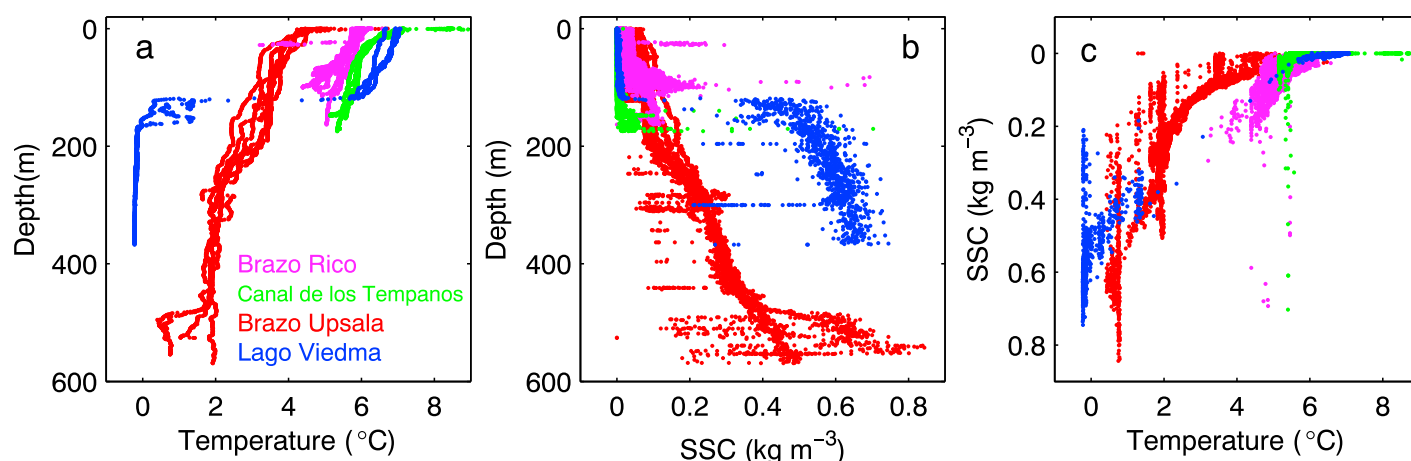
Figure 11. Individual data obtained by the temperature, turbidity, and depth profiler plotted for (a) depth versus temperature, (b) depth versus SSC, and (c) SSC versus temperature.

significant change at this same depth (Figures 10g and 10h). The pycnocline was at the depth of 120 m, which is close to the bed elevation at the sill found at 2 km from the ice front (Figures 4c and 9d). Below this level, water mass shows the coldest temperature and the highest SSC among the data obtained in this study (Figures 11a and 11b). We assume that highly turbid water discharged from the glacier bed filled the basin formed between the ice front and the sill. Within this lower layer, SSC shows high-frequency variations and the Brund-Väisälä frequency is negative at several depths (Figure 10h). Thus, subglacial discharge from GV stimulates mixing within the lower layer and excess water flows over the sill to the main lake basin. The ablation area of GV is 40% greater than that of GU, and thus a greater amount of subglacial discharge is expected. In contrast to the meltwater, ice discharge from GV is relatively small because the calving front is narrower than the other two glaciers and ice speed is < 30% of GU. Because ice flux is relatively small and the glacier front is in contact with the main basin of LV, the upper layer showed the warmest temperature among the lakes studied (Figure 11a). It is most likely that wind-driven water mixing extends down to the thermocline at a depth of 120 m, and this mixing keeps the temperature within the upper layer fairly uniform.

The thermal structure of LV suggests its important influence on glacier ablation at the calving front. Our measurements revealed that the lower half of the calving cliff is in contact with cold water at the pressure melting point (Figures 8b and 9d). Melting is very slight on such an interface, and thus the contribution of subaqueous melting to the frontal ablation should be minor. It implies that the ice in contact with the cold water tends to protrude into the lake, slowly melts, and detaches from the glacier by subaqueous calving. Formation of subaqueous ice ramps extending from glacier fronts was observed in proglacial lakes in New Zealand [*Robertson et al.*, 2012].

5.2. Subaqueous Ice Melting

The thermal structure of the lakes revealed in this study has important implications for subaqueous ice melting at the calving front. First, since subglacial discharge does not form an upwelling plume in front of freshwater calving glaciers, the regime of heat exchange at the ice-water interface is significantly different from that of tidewater glaciers. Glacial meltwater upwells in front of a tidewater glacier, drawing warm ocean water into a plume. This entrainment of warm water increases subaqueous melt rate by facilitating efficient heat exchange between the ice cliff and ocean water [*Motyka et al.*, 2003, 2013; *Rignot et al.*, 2010; *Jenkins*, 2011; *Xu et al.*, 2013]. In the proglacial lakes in Patagonia, wind-driven water mixing is active down to a depth of ~100–200 m. It is likely that heat from solar radiation is transported by this process from the surface to deeper regions, providing heat for ice melting.

Second, our measurements in BU and LV showed that the lower part of the calving cliff interfaces with cold water (Figures 9c and 9d). Melting is very slight in this region, particularly at the lower half of the GV calving front, which is in contact with water at pressure melting point (Figure 9d). It is commonly accepted that
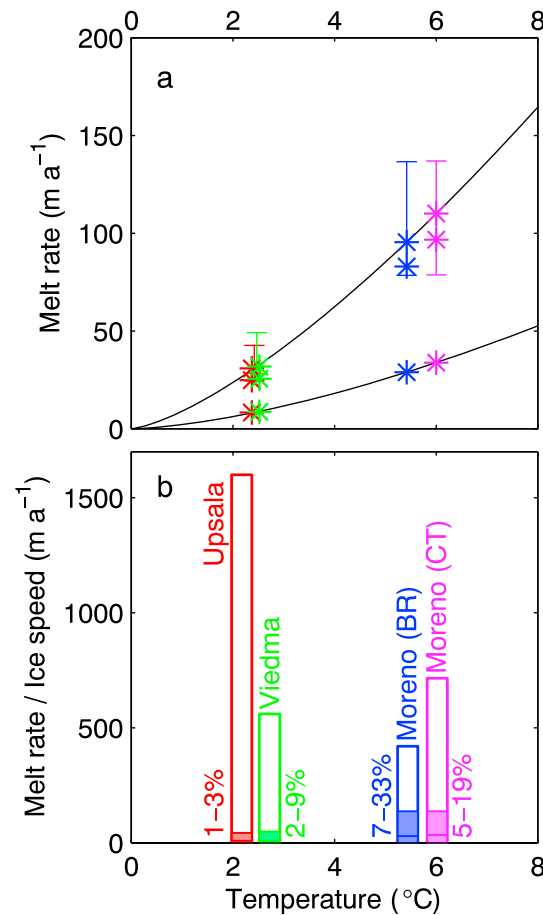
Figure 12. (a) Subaqueous melt rates estimated from water temperature measured in each lake. The asterisks were obtained from equations (2)–(4), and the ranges given by the vertical lines from equation (5) with water current assumed as 0.1–0.2 m s^{-1}. The upper and lower curves are melt rates computed using equations (3) and (4), respectively. (b) Ice flow speed at the glacier front (open column) compared with the estimated melt rate (shaded). The numbers indicate the ranges of proportion of the melt rates to the ice speed.

overdeepened bed geometry affects ice dynamics and plays a key role in frontal variations of a calving glacier [e.g., *Nick et al.,* 2009]. In the case of freshwater calving glaciers, ponding of cold water within an overdeepened basin provides another mechanism by which basal depression can impact ice dynamics.

Data presented in this study are insufficient to accurately quantify the melting of calving fronts in lakes. However, estimation of subaqueous melt rate is possible from the water temperature profiles by using empirical relationships reported in previous studies. Here we employ several equations proposed for iceberg melting [*Weeks and Campbell,* 1973; *Neshyba and Josberger,* 1980; *Russell-Head,* 1980; *Sakai et al.,* 2009].

$$m = 1.8 \times 10^{-2} \Delta T^{1.5} \quad (m \ d^{-1}) \tag{2}$$

$$m = 2.45 \times 10^{-2} \Delta T^{1.4} \quad (m \ d^{-1}) \tag{3}$$

$$m = 2.14 \ \Delta T^{1.54} \quad (m \ a^{-1}) \tag{4}$$

$$m = 7.14 \times 10^{-6} v^{0.8} \frac{\Delta T}{l^{0.2}} \quad (m \ s^{-1}) \tag{5}$$

Equations (2)–(4) relate subaqueous melt rate m with water temperature above freezing ΔT (°C). These are empirical relationships based on laboratory experiments and iceberg observations. Equation (5) includes water current v (m s^{-1}) and length of ice-water interface l (m) as additional variables, which was derived for ice plate melting in saline water by *Weeks and Campbell* [1973] and later adopted for freshwater melting by *Sakai et al.* [2009]. We took water temperature profiles obtained near the center of the glacier fronts and averaged the temperature from the surface to the bottom to substitute ΔT. Water current was assumed to be within a range of 0.1–0.2 m s^{-1} as a first estimate. The length of ice-water interface was approximated by the water depth at the location of the temperature measurement, assuming vertical water circulation along the ice front. With these values, equations (2)–(5) give melt rates of 29–137 m a^{-1} for GPM in BR, 34–137 m a^{-1} for GPM in CT, 8–43 m a^{-1} for GU, and 9–49 m a^{-1} for GV (Figure 12a). To evaluate the contribution of melting to the frontal ablation of the glaciers, the melt rates were compared with the ice speed at the calving front (Figure 12b). Speed averaged along each calving front of GPM [*Stuefer et al.,* 2007], and 80% of speed at the glacier center near the terminus of GU and GV [*Sakakibara and Sugiyama,* 2014] were used for this purpose. The calculated melt rates correspond to 7–33% and 5–19% of the ice speed of GPM in BR and CT, respectively. The fraction is smaller in GU (1–3%) and GV (2–9%). These results suggest a relatively small contribution of melting to frontal ablation at the studied glaciers; i.e., ice is lost mostly by calving. However, our field observations indicate that subaqueous calving is not commonly observed on these glaciers. For example, according to time lapse photography at the front of GPM in BR from December 2014 to January 2015, only 2% out of 364 calving events occurred in the water [*Minowa et al.,* 2016].
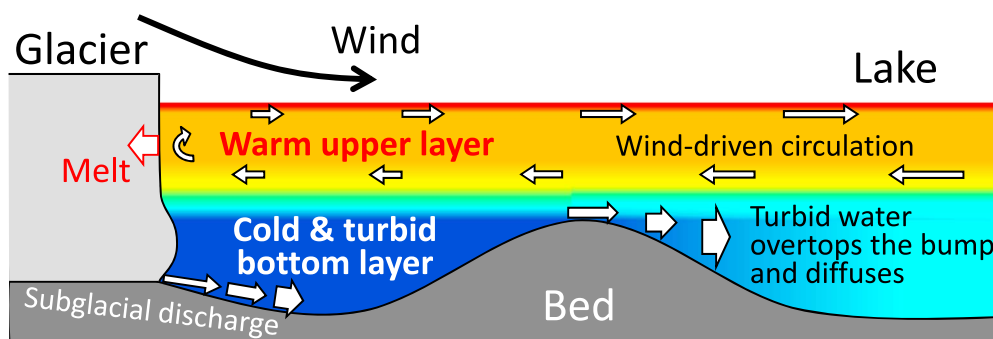
Figure 13. Schematic diagram showing the thermal structure of a lake in front of a calving glacier based on the observations in this study.

Water current is one of the most important unknown variables in the melt rate calculations. *Sakai et al.* [2009] performed numerical experiments on wind and water current in front of a lake calving glacier and reported that wind-generated vertical water current reached $0.5\,\mathrm{m\,s}^{-1}$ at the glacier front. If we apply this current speed to equation (5), the contribution of melting to frontal ablation is 70%, 40%, 6%, and 18% at GPM-BR, GPM-CT, GU, and GV, respectively. Another shortcoming of the above calculation is water temperature averaged over the depth. Because lakewater temperature showed large variations in depth, the melt rate is expected to be inhomogeneous. It is likely that the shape of ice in water may be complex, which affects water circulation and melting. Therefore, measurements of water current near the ice front together with observations of the calving front shape within the water are needed to understand better the frontal melting of freshwater calving glaciers. Numerical modeling of lake water circulation also helps more accurate melt rate estimation, and such a model should include the effect of sediment concentration on water density and the influence of lake bed geometry on water movement. Accurate understanding of these processes and inclusion of the processes in calving glacier models are crucial to predict the future evolution of freshwater calving glaciers in Patagonia and other regions of the world.

6. Conclusions

To better understand the interactions of freshwater calving glaciers and proglacial lakes, lakewater properties and bathymetry measurements were performed near the front of three major calving glaciers in the SPI. A water temperature and turbidity profiler was lowered to the lake bottom from a boat equipped with an ultrasonic echo sounder. Temperature distributions of lake water were analyzed from the observations carried out, and the influence of subglacial discharge and lake bed geometry on the thermal structure was investigated.

In front of GPM, both BR and CT were characterized by relatively warm and clean water. Water properties were uniformly distributed from the surface to the ~180 m deep bottom without clear stratifications. The spatially uniform water properties imply that wind-driven vertical mixing extends to the lake bottom. It is likely that this mixing plays a role in transporting heat from near surface to the ice-water interface. In BU, ~600 m deep lake water consisted of three isothermal layers: relatively warm near-surface water (3–4°C, 40–180 m), intermediate water (~2°C, 280–470 m), and cold bottom water (<1°C, >490 m). Water was more turbid in deeper layers, suggesting the influence of subglacial meltwater discharge. This result indicates that turbid and cold meltwater remains at the deeper region after the discharge because sediment concentration is the dominant control of the water density. Near the front of GV, very clear two-layer stratification was observed in LV. Water was clean and warm (6–7°C) at 0–120 m, whereas turbid and very cold (nearly equal to the pressure melting point) water was found below 120 m. The thermocline was located at a similar depth as the sill observed at a distance of 2 km from the glacier front. Our interpretation is that turbid and cold glacial discharge fills the entire region below the thermocline, because the sill acts as a dam for this dense meltwater.

Our observations revealed the thermal structure of lakes in front of large calving glaciers, which are significantly different from those of tidewater glaciers in fjords. Important features of the lake thermal structure are illustrated in Figure 13. Wind-driven circulation is efficient enough to mix the upper ~180 m, which conveys heat to the calving front. Nevertheless, cold glacial water fills the regions near the lake bottom, resulting

in no efficient heat transfer to the deeper part of the ice-water interface. This is because turbid glacial water is denser than ambient lake water, and thus subglacial discharge does not form an upwelling current. Lake bed geometry affects the thermal structure as well, because turbid and cold meltwater remains in a bed depression until it overtops a bedrock bump and diffuses to the lower reaches. Crude estimate of subaqueous melt rates using previously proposed empirical relationships between the melt rate and water temperature showed that melting accounts for ~5–30% of the frontal ablation at GPM. In the case of GU and GV, it accounts for only a limited portion (<10%) because of the cold lake water and greater amount of ice discharge into the lake. For a more accurate understanding of the frontal ablation in freshwater calving glaciers, further detailed investigations are required of the processes that occur at the ice-water boundary.

References

Aniya, M. (1988), Glacier inventory for the Northern Patagonia Icefield, Chile, and variations 1944/45 to 1985/86, *Arct. Alp. Res.*, *20*(2), 179–187.

Aniya, M., H. Sato, R. Naruse, P. Skvarca, and G. Casassa (1996), The use of satellite and airborne imagery to inventory outlet glaciers of the Southern Patagonia Icefield, South America, *Photogramm. Eng. Remote Sens.*, *62*(12), 1361–1369.

Aniya, M., H. Sato, R. Naruse, P. Skvarca, and G. Casassa (1997), Recent glacier variations in the Southern Patagonia Icefield, South America, *Arct. Alp. Res.*, *29*(1), 1–12.

Bartholomaus, T. C., C. F. Larsen, and S. O'Neel (2013), Does calving matter? Evidence for significant submarine melt, *Earth Planet. Sci. Lett.*, *380*, 21–30.

Boyce, E. S., R. J. Motyka, and M. Truffer (2007), Flotation and retreat of a lake-calving terminus, Mendenhall Glacier, southeast Alaska, USA, *J. Glaciol.*, *53*(181), 211–224.

Carrivick, J. L., and D. J. Quincey (2014), Progressive increase in number and volume of ice-marginal lakes on the western margin of the Greenland Ice Sheet, *Global Planet. Change*, *116*, 156–163.

Carrivick, J. L., and F. S. Tweed (2013), Proglacial lakes: Character, behaviour and geological importance, *Quat. Sci. Rev.*, *78*, 34–52.

Chikita, K. A. (2007), Topographic effects on the thermal structure of Himalayan glacial lakes: Observations and numerical simulation of wind, *J. Asian Earth Sci.*, *30*, 344–352.

Chikita, K. A., N. D. Smith, N. Yonemitsu, and M. Perez-Arlugea (1996), Dynamics of sediment-laden underflows passing over a subaqueous sill: Glacier-fed Peyto Lake, Alberta, Canada, *Sedimentology*, *43*(5), 865–875.

Chikita, K., J. Jha, and T. Yamada (1999), Hydrodynamics of a supraglacial lake and its effect on the basin expansion: Tso Rolpa, Rolwaling Valley, Nepal Himalaya, *Arct. Antarct. Alp. Res.*, *31*(1), 58–70.

Ciappa, A., L. Pietranera, and F. Battazza (2010), Perito Moreno Glacier (Argentina) flow estimation by COSMO SkyMed sequence of high-resolution SAR-X imagery, *Remote Sens. Environ.*, *114*, 2088–2096.

Davies, B. J., and N. F. Glasser (2012), Accelerating shrinkage of Patagonian glaciers from the Little Ice Age (AD 1870) to 2011, *J. Glaciol.*, *58*(212), 1063–1083.

De Angelis, H. (2014), Hypsometry and sensitivity of the mass balance to changes in equilibrium-line altitude: The case of the Southern Patagonia Icefield, *J. Glaciol.*, *60*(219), 14–28.

Fujita, K., A. Sakai, S. Takenaka, T. Nuimura, A. B. Surazakov, T. Sawagaki, and T. Yamanokuchi (2013), Potential flood volume of Himalayan glacial lakes, *Nat. Hazards Earth Syst. Sci.*, *13*, 1827–1839.

Funk, M., and H. Röthlisberger (1989), Forecasting the effects of a planned reservoir which will partially flood the tongue of Unteraargletscher, *Ann. Glaciol.*, *13*, 76–81.

Gladish, C. V., D. M. Holland, A. Rosing-Asvid, J. W. Behrens, and J. Boje (2015), Oceanic boundary conditions for Jakobshavn Glacier. Part I: Variability and renewal of Ilulissat Icefjord waters, 2001–14, *J. Phys. Oceanogr.*, *45*(1), 3–32.

Haresign, E., and C. A. Warren (2005), *Melt Rates at Calving Termini: A Study at Glacier Leon, Chilean Patagonia*, *Spec. Publ.*, vol. 242, pp. 99–109, Geol. Soc., London.

Hochstein, M. P., D. Claridge, S. A. Henrys, A. Pyne, D. C. Nobes, and S. F. Leary (1995), Downwasting of the Tasman Glacier (South Island, N.Z.): Changes in the terminus region between 1971 and 1993, *N. Z. J. Geol. Geophys.*, *38*(1), 1–16.

Hochstein, M. P., M. I. Watson, B. Malengrenau, D. C. Nobes, and I. Owens (1998), Rapid melting of the terminal section of the Hooker Glacier (Mt Cook National Park, New Zealand), *N. Z. J. Geol. Geophys.*, *41*(3), 203–218.

Inall, M. E., T. Murray, F. R. Cottier, K. Scharrer, T. J. Boyd, K. J. Heywood, and S. L. Bevan (2014), Oceanic heat delivery via Kangerdlugssuaq Fjord to the south-east Greenland ice sheet, *J. Geophys. Res. Oceans*, *119*, 631–645, doi:10.1002/2013JC009295.

Jackson, R. H., F. Straneo, and D. A. Sutherland (2014), Externally forced fluctuations in ocean temperature at Greenland glaciers in non-summer months, *Nat. Geosci.*, *3*, 182–186.

Jenkins, A. (2011), Convection-driven melting near the grounding lines of ice shelves and tidewater glaciers, *J. Phys. Oceanogr.*, *41*(12), 2279–2294.

Josberger, E. G., R. A. Shuchman, G. A. Meadows, S. Savage, and J. Payne (2006), Hydrography and circulation of ice-marginal lakes at Bering Glacier, Alaska, U.S.A, *Arct. Antarct. Alp. Res.*, *38*(4), 547–560.

Larsen, C. F., R. J. Motyka, A. A. Arendt, K. A. Echelmeyer, and P. E. Geissler (2007), Glacier changes in southeast Alaska and northwest British Columbia and contribution to sea level rise, *J. Geophys. Res.*, *112*, F01007, doi:10.1029/2006JF000586.

Larsen, C. F., E. Burgess, A. A. Arendt, S. O'Neel, A. J. Johnson, and C. Kienholz (2015), Surface melt dominates Alaska glacier mass balance, *Geophys. Res. Lett.*, *42*, 5902–5908, doi:10.1002/2015GL064349.

McNabb, R. W., and R. Hock (2014), Alaska tidewater glacier terminus positions, 1948–2012, *J. Geophys. Res. Earth Surf.*, *119*, 153–167, doi:10.1002/2013JF002915.

Minowa, M., S. Sugiyama, D. Sakakibara, and T. Sawagaki (2015), Contrasting glacier variations of Glaciar Perito Moreno and Glaciar Ameghino, Southern Patagonia Icefield, *Ann. Glaciol.*, *56*(70), 26–32.

Minowa, M., S. Sugiyama, D. Sakakibara, E. Podolskiy, Y. Ohashi, and P. Skvarca (2016), High-frequency surface wave measurements of micro-tsunamis generated by Glacier Calving, Geophys. Res. Abstract, 18, EGU2016-1852.

Moon, T., and I. Joughin (2008), Changes in ice front position on Greenland's outlet glaciers from 1992 to 2007, *J. Geophys. Res.*, *113*, F02022, doi:10.1029/2007JF000927.

Motyka, R. J., L. Hunter, K. A. Echelmeyer, and C. Connor (2003), Submarine melting at the terminus of a temperate tidewater glacier, LeConte Glacier, Alaska, U.S.A, *Ann. Glaciol.*, *36*, 57–65.

Motyka, R. J., W. P. Dryer, J. Amundson, M. Truffer, and M. Fahnestock (2013), Rapid submarine melting driven by subglacial discharge, LeConte Glacier, Alaska, *Geophys. Res. Lett.*, *40*, 5153–5158, doi:10.1002/grl.51011.

Muto, M., and M. Furuya (2013), Surface velocities and ice-front positions of eight major glaciers in the Southern Patagonian Ice Field, South America, from 2002 to 2011, *Remote Sens. Environ.*, *139*, 50–59.

Naruse, R., and P. Skvarca (2000), Dynamic features of thinning and retreating Glaciar Upsala, a lacustrine calving glacier in southern Patagonia, *Arct. Antarct. Alp. Res.*, *32*(4), 485–491.

Neshyba, S., and E. G. Josberger (1980), On the estimation of Antarctic iceberg melt rate, *J. Phys. Oceanogr.*, *10*, 1681–1685.

Nick, F. M., A. Vieli, I. M. Howat, and I. Joughin (2009), Large scale changes in Greenland outlet glacier dynamics triggered at the terminus, *Nat. Geosci.*, *2*(2), 110–114.

Nie, Y., Q. Liu, and S. Liu (2013), Glacial lake expansion in the central Himalayas by Landsat images, 1990–2010, *PLoS One*, *8*(12), e83973.

Pasquini, A. I., and P. J. Depetris (2011), Southern Patagonia's Perito Moreno Glacier, Lake Argentino, and Santa Cruz River hydrological system: An overview, *J. Hydrol.*, *405*, 48–56.

Petrenko, V. F., and R. W. Whitworth (1999), *Physics of Ice*, pp. 373 , Oxford Univ. Press, Oxford, U. K.

Rignot, E., A. Rivera, and G. Casassa (2003), Contribution of the Patagonia Icefields of South America to sea level rise, *Science*, *302*(6544), 434–437.

Rignot, E., M. Koppes, and I. Velicogna (2010), Rapid submarine melting of the calving faces of West Greenland glaciers, *Nat. Geosci.*, *3*(3), 187–191.

Rivera, A., and G. Casassa (1999), Volume changes on Pío XI glacier, Patagonia, 1975–1995, *Global Planet. Change*, *22*, 233–244.

Robertson, C. M., D. I. Benn, M. S. Brook, I. C. Fullier, and K. A. Holt (2012), Subaqueous calving margin morphology at Mueller, Hooker and Tasman glaciers in Aoraki/Mount Cook National Park, New Zealand, *J. Glaciol.*, *58*(212), 1037–1046.

Rott, H., M. Stuefer, A. Siegel, P. Skvarca, and A. Eckstaller (1998), Mass fluxes and dynamics of Moreno Glacier, Southern Patagonia Icefield, *Geophys. Res. Lett.*, *25*, 1407–1410, doi:10.1029/98GL00833.

Russell-Head, D. S. (1980), The melting of free-drifting icebergs, *Ann. Glaciol.*, *1*, 119–122.

Sakai, A., K. Nishimura, T. Kadota, and N. Takeuchi (2009), Onset of calving at supraglacial lakes on debris-covered glaciers of the Nepal Himalaya, *J. Glaciol.*, *55*(193), 909–917.

Sakakibara, D., and S. Sugiyama (2014), Ice-front variations and speed changes of calving glaciers in the Southern Patagonia Icefield from 1984 to 2011, *J. Geophys. Res. Earth Surf.*, *119*, 2541–2554, doi:10.1002/2014JF003148.

Sakakibara, D., S. Sugiyama, T. Sawagaki, S. Marinsek, and P. Skvarca (2013), Rapid retreat, acceleration, and thinning of Glaciar Upsala in the Southern Patagonia Icefield, initiated in 2008, *Ann. Glaciol.*, *54*(63), 131–138.

Sciascia, R., F. Straneo, C. Cenedese, and P. Heimbach (2013), Seasonal variability of submarine melt rate and circulation in an East Greenland fjord, *J. Geophys. Res. Oceans*, *118*, 2492–2506, doi:10.1002/jgrc.20142.

Skvarca, P., and R. Naruse (1997), Dynamic behavior of Glaciar Perito Moreno, southern Patagonia, *Ann. Glaciol.*, *24*, 268–271.

Skvarca, P., and R. Naruse (2006), Overview of the ice-dam formation and collapse of Glaciar Perito Moreno, southern Patagonia, in 2003/4, *J. Glaciol.*, *52*(177), 476–478.

Straneo, F., G. S. Hamilton, D. A. Sutherland, L. A. Stearns, F. Davidson, M. O. Hammill, G. B. Stenson, and A. Rosing-Asvid (2010), Rapid circulation of warm subtropical waters in a major glacial fjord in East Greenland, *Nat. Geosci.*, *3*, 182–186.

Stuefer, M. (1999), Investigations on mass balance and dynamics of Moreno Glacier based on field measurements and satellite imagery, Ph.D. thesis, 166 pp., Universität Innsbruck.

Stuefer, M., H. Rott, and P. Skvarca (2007), Glaciar Perito Moreno, Patagonia: Climate sensitivities and glacier characteristics preceding the 2003/04 and 2005/06 damming events, *J. Glaciol.*, *53*(180), 3–16.

Sugiyama, S., P. Skvarca, N. Naito, H. Enomoto, S. Tsutaki, K. Tone, S. Marinsek, and M. Aniya (2011), Ice speed of a calving glacier modulated by small fluctuations in basal water pressure, *Nat. Geosci.*, *4*(9), 597–600.

Sutherland, D. A., and F. Straneo (2012), Estimating ocean heat transports and submarine melt rates in Sermilik Fjord, Greenland, using lowered acoustic Doppler current profiler (LADCP) velocity profiles, *Ann. Glaciol.*, *53*(60), 50–58.

Truffer, M., and R. J. Motyka (2016), Where glaciers meet water: Subaqueous melt and its relevance to glaciers in various settings, *Rev. Geophys.*, *54*, 220–239, doi:10.1002/2015RG000494.

Trüssel, B. L., R. J. Motyka, M. Truffer, and C. F. Larsen (2013), Rapid thinning of lake-calving Yakutat Glacier and the collapse of the Yakutat Icefield, southeast Alaska, USA, *J. Glaciol.*, *59*(213), 149–161.

Warren, C., and M. P. Kirkbride (2003), Calving speed and climatic sensitivity of New Zealand lake-calving glaciers, *Ann. Glaciol.*, *36*(1), 173–178, doi:10.3189/172756403781816446.

Weeks, W. F., and W. J. Campbell (1973), Icebergs as a freshwater source: An appraisal, *J. Glaciol.*, *12*(65), 207–232.

White, A., and L. Copland (2015), Decadal-scale variations in glacier area changes across the Southern Patagonian Icefield since the 1970s, *Arct. Antarct. Alp. Res.*, *47*(1), 147–167.

Willis, M. J., A. K. Melkonian, M. E. Pritchard, and A. Rivera (2012), Ice loss from the Southern Patagonian Ice Field, South America, between 2000 and 2012, *Geophys. Res. Lett.*, *39*, L17501, doi:10.1029/2012GL053136.

Xu, Y., E. Rignot, I. Fenty, D. Menemenlis, and M. M. Flexas (2013), Subaqueous melting of Store Glacier, west Greenland from three-dimensional, high-resolution numerical modeling and ocean observations, *Geophys. Res. Lett.*, *40*, 4648–4653, doi:10.1002/grl.50825.